Artifacts Extraction from EEG Data Using the Infomax Approach

JOANNA GÓRECKA[1,*], PIOTR WALERJAN[2]

[1]*Department of Systems Engineering, Signals and Electronics,*
West Pomeranian University of Technology, Szczecin, Poland
[2]*PWSIM MEDISOFT, Warsaw, Poland*

The aim of the research is to detect and remove undesired components from EEG data by means of ICA approach. Besides classical signal analysis tools such as adaptive supervised filtering, parametric or non-parametric spectral estimation, time-frequency analysis, the proposed ICA technique can be used for detection of a wide group of artifacts from EEG data. In this paper a new form of nonlinearity implemented in the infomax approach is presented. As it has been proven experimentally, the proposed new sigmoidal function can effectively detect the selected group of artifacts from EEGs and is an useful approach to speed up computations.

K e y w o r d s: Independent Component Analysis, infomax algorithm, sigmoidal function, EEG data, artifacts

1. Introduction

The Electroencephalogram is a biological signal recorded at the scalp and represents electrical activity of the brain. The analysis and extraction of information from the EEG data is a difficult problem, because these low amplitude signals are distorted by different undesired components – artifacts and noise [1].

The EEG artifacts may be divided into two groups depending on their origin: physiological artifacts or technical artifacts [2]. Eye movements, ECG, EMG, pulse, sweating, patient's body movements are examples of the biological artifacts. 50 Hz line noise, static electricity discharges, movements of electrode leads are examples of the technical artifacts. Generally, artifacts should be removed from the recording by the technician performing the EEG examination, but it is not always possible.

Many methods have been proposed to remove the most popular artifact: eye blinks, muscle activity or line noise from EEG data, including methods that use frequency – band filtering technique and methods based on regression or principal component analysis (PCA) [2, 3]. In practice, any frequency component above 100 Hz is removed with lowpass filters, because the routine EEG recordings contain data below this value. In cases, where the EEG data acquisition system is unable to cancel out line frequency, a notch filter is used. However, these methods lead to considerable loss in collected information. For that reason it has been proposed the ICA approach.

Generally, the choice of adaptive algorithm depends on statistical properties of the source signals. The assumption of independence and nongaussianity of the EEG signals was justified through the successful application of the ICA approach to the detection and extraction of selected artifacts in EEG data [3–10]. The algorithms for separation of artifacts from EEG data can be divided into two categories: adaptive and batch mode algorithms [5].

In the first category the adaptive algorithms often are based on stochastic gradient methods. The main problem of the adaptive gradient algorithms is the slow convergence, which can be improved using the natural gradient method and dependence on the correct choice of the learning rate parameters in neural networks [5]. In the case, where all the independent components are estimated at the same time, an extended infomax algorithm is used to maximize the output entropy [6, 7].

In the second category, where all the computations are made in batch mode, the tensor based methods and algorithm based on a fixed point iteration are available, for example: the JADE algorithm (Joint Approximate Diagonalization of Eigenmatrices), which diagonalizes the fourth-order cumulant of the estimated sources [3, 8] or the FastICA algorithm based on maximizing the negentropy or kurtosis [6, 9]. For computational reasons, the tensor based methods cannot be used in larger dimensions. FastICA can be used for extracting the independent components one-by-one only on basis of their kurtosis and is a much faster algorithm than that given by the gradient method. It is used for separation of the EEG data with good accuracy, but corrupted only by eye and muscle artifacts.

A different method for the artifacts separation exploits nonstationarity of the EEG signals, i.e. SOBI (Second-Order Blind Identification). This algorithm is based on second-order statistics and separates temporally correlated sources. Mostly, it is used for extraction of the ocular artifacts [3, 10].

2. Method

For the artifacts removal we propose the infomax approach. It has been proven that, for separation of the EEG data, the best performance can by achieved using the infomax rule [7, 11]. Sigmoid functions used in the infomax algorithms, e.g. the logistic

sigmoid $g_1(\mathbf{u}) = \dfrac{1}{1 + \exp^{-\mathbf{u}}}$ or the hyperbolic sigmoid $g_2(\mathbf{u}) = \tanh(\mathbf{u})$, provide *a priori* knowledge about the source distribution. In ideal case, the form of nonlinearity should be the cumulative density function of distributions of the independent sources:

$p(s_i) = p(u_i) = \left| \dfrac{\partial g(u_i)}{\partial u_i} \right|$. The first form of the natural gradient infomax algorithm [12] can be written as:

$$\Delta \mathbf{W} \propto \frac{\partial H(\mathbf{y})}{\partial \mathbf{W}} \mathbf{W}^T \mathbf{W} = \left[\mathbf{I} + \varphi(\mathbf{u}) \mathbf{u}^T \right] \mathbf{W},\tag{1}$$

where $\varphi(\mathbf{u})$ is the gradient vector of log likelihood called the score function defined as relation between the probability density function of $\mathbf{u}$ and its derivative:

$$\varphi(\mathbf{u}) = \frac{\dfrac{\partial p(\mathbf{u})}{\partial \mathbf{u}}}{p(\mathbf{u})} = \left[\frac{\dfrac{\partial p(u_1)}{\partial u_1}}{p(u_1)}, ..., \frac{\dfrac{\partial p(u_N)}{\partial u_N}}{p(u_N)} \right]^T,\tag{2}$$

$p(\mathbf{u}) = \prod_{i=1}^{N} p(u_i)$ is the hypothesized distribution of $p(\mathbf{s})$. The presented algorithm that uses a logistic sigmoid was implemented in [13] for separation of the EEG signals. However, it is limited to extracting of sources with the supergaussian distributions only.

In the normal brain activity the EEG data have the supergaussian distributions. Furthermore, a high positive normalized kurtosis value (higher than 5) indicates an abnormal brain activity, e.g. an epileptic seizure and nonepileptic attacks, event-related potentials or any physiological artifacts. It is worth to note, that the non-physiological artifacts and the slow brain activity have the subgaussian distributions. Therefore, for separation of the EEG data an extended infomax algorithm has been proposed [6], which can separate both types of distributions using a parametric density model:

$$\Delta \mathbf{W} \propto \frac{\partial H(\mathbf{y})}{\partial \mathbf{W}} \mathbf{W}^T \mathbf{W} = \left[\mathbf{I} - \mathbf{K} \tanh(\mathbf{u}) \mathbf{u}^T - \mathbf{u}\mathbf{u}^T \right] \mathbf{W},\tag{3}$$

where: $\mathbf{K}$ is N – dimensional diagonal matrix with the k_{ii} elements. For supergaussian sources $k_{ii} = 1$ and for subgaussian sources $k_{ii} = -1$. In this algorithm, the subgaussian distributions can be modelled with a symmetrical form of the Pearson mixture model and the supergaussian distributions can be modelled as derivative of the hyperbolic tangent. The following switching criterion between the sub- and supergaussian learning rule was used [6]:

$$k_{ii} = \text{sign}\left(E\left\{\text{sech}^2\left(u_i\right)\right\}E\left\{u_i^2\right\} - E\left\{\tanh\left(u_i\right)u_i\right\}\right). \qquad (4)$$

The learning rule given by eq. 3 is the final version of the infomax approach implemented in the EEGLAB toolbox [13].

In [14] it has been presented a general form of the extended infomax algorithm, where it is assumed that $\varphi(\mathbf{u}) < 0$, which means $\dfrac{\dfrac{\partial^2 g(\mathbf{u})}{\partial \mathbf{u}^2}}{\dfrac{\partial g(\mathbf{u})}{\partial \mathbf{u}}} < 0$. Theoretically, this assumption is allowed to choose the optimal nonlinearity $g(\mathbf{u})$ for separation of different nongaussian distributions [14]. The proposition of the general form of the extended infomax algorithm is written as:

$$\Delta\mathbf{W} \propto \frac{\partial H(\mathbf{y})}{\partial \mathbf{W}}\mathbf{W}^T\mathbf{W} = \left[\mathbf{I} - k\varphi(\mathbf{u})\mathbf{u}^T - \mathbf{u}\mathbf{u}^T\right]\mathbf{W}, \qquad (5)$$

where k can be derived from the stability analysis of separating signals [6] or can be the sign of normalized kurtosis [12].

For the EEG signal separation we propose a new form of nonlinearity implemented in the infomax approach presented in eq. 5. The new nonlinear function is given by:

$$g_{bip}(\mathbf{u}) = \frac{\mathbf{u}}{1 + \sqrt{b + \mathbf{u}^2}}, \qquad (6)$$

where the coefficient b is the slope parameter. Shape of the new function for different values of the slope parameter is presented in Fig. 1. The proposed nonlinearity
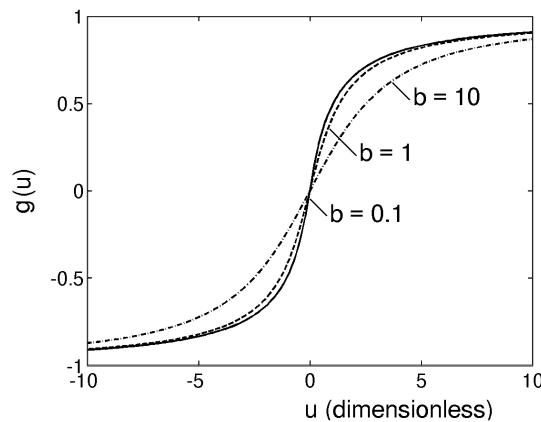
Fig. 1. Algebraic bipolar sigmoid function $g_{bip}(\mathbf{u}) = \dfrac{\mathbf{u}}{1 + \sqrt{b + \mathbf{u}^2}}$ for different values of the slope parameter b, $\mathbf{u}$ is a vector
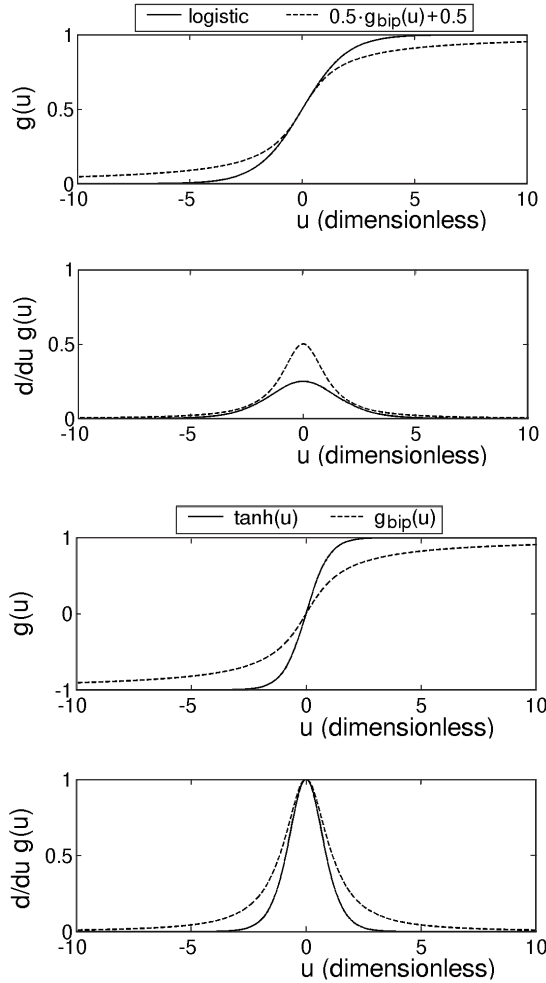
Fig. 2. Comparison of the typical transfer functions and their derivatives: logistic sigmoid $g_1(\mathbf{u}) = \dfrac{1}{1 + \exp^{-\mathbf{u}}}$, hyperbolic sigmoid $g_2(\mathbf{u}) = \tanh(\mathbf{u})$, and the proposed new bipolar nonlinearity $g_{bip}(\mathbf{u}) = \dfrac{\mathbf{u}}{1 + \sqrt{b + \mathbf{u}^2}}$ with its unipolar form: $g_{uni}(\mathbf{u}) = 0.5 \cdot g_{bip}(\mathbf{u}) + 0.5$, $\mathbf{u}$ is a vector

is an algebraic bipolar sigmoid function that belongs to the type of the simple sigmoids and satisfies their conditions [15]. This function is applied for separation of two types of the EEG signal distributions, i.e. subgaussians (i.e. platykurtic, normalized kurtosis < 0) and supergaussians (i.e. leptokurtic, normalized kurtosis > 0). The proposed function can be linearly transformed to obtain output between 0 and 1, i.e. $g_{uni}(\mathbf{u}) = 0.5 \cdot g_{bip}(\mathbf{u}) + 0.5$, which is shown in Fig. 2. The form of the score function $\varphi(\mathbf{u})$ depends on the type of the nonlinear function and the

value of the slope parameter. Hence, for $b > 0$, the score function is defined as:

$$\varphi(\mathbf{u}) = -\frac{g_{bip2}(\mathbf{u})_{|b>0}}{b + \mathbf{u}^2}\left[3b + 2\mathbf{u}g_{bip}(\mathbf{u})_{|b>0}\right], \text{ where } g_{bip2}(\mathbf{u}) = \frac{\mathbf{u}}{b + \sqrt{b + \mathbf{u}^2}} \text{ is another}$$

new bipolar function. Now, the extended infomax algorithm can by written in the following form:

$$\Delta\mathbf{W} \propto \frac{\partial H(\mathbf{y})}{\partial\mathbf{W}}\mathbf{W}^T\mathbf{W} = \left[\mathbf{I} - \text{sign}(k)\frac{g_{bip}(\mathbf{u})_{|b>0}}{b + \mathbf{u}^2}\left(3b + 2\mathbf{u}g_{bip}(\mathbf{u})_{|b>0}\right)\mathbf{u}^T - \mathbf{u}\mathbf{u}^T\right]\mathbf{W}. \quad (7)$$

On the other hand, by putting $b = 1$ the score function reduces to

$$\varphi(\mathbf{u}) = -\frac{g_{bip}(\mathbf{u})_{|b=1}}{1 + \mathbf{u}^2}\left[3 + 2\mathbf{u}g_{bip}(\mathbf{u})_{|b=1}\right] \text{ and the learning algorithm can be for-}$$

mulated as the following form:

$$\Delta\mathbf{W} \propto \frac{\partial H(\mathbf{y})}{\partial\mathbf{W}}\mathbf{W}^T\mathbf{W} = \left[\mathbf{I} - \text{sign}(k)\frac{g_{bip}(\mathbf{u})_{|b=1}}{1 + \mathbf{u}^2}\left(3 + 2\mathbf{u}g_{bip}(\mathbf{u})_{|b=1}\right)\mathbf{u}^T - \mathbf{u}\mathbf{u}^T\right]\mathbf{W}. \quad (8)$$

The switching criterion for the new proposition of the adaptive learning infomax rule is the sign of the normalized kurtosis ($k < 0$ for the subgaussian distributions, $k > 0$ for the supergaussian distributions). The presented new learning rule satisfies the sufficient condition that guarantees asymptotic stability [16], i.e. $\kappa_i > 0$, where $\kappa_i = E\{\varphi_i'(u_i)\}E\{u_i^2\} - E\{\varphi_i(u_i)u_i\}$. For the new infomax rule the asymptotic stability is always guaranteed, because:

$$\kappa_i = E\left\{u_i^2\frac{\left(3 + \sqrt{1 + u_i^2}\right)\left(2u_i^4 - 3\right)}{\left(\sqrt{1 + u_i^2}\right)^5\left(1 + \sqrt{1 + u_i^2}\right)^4} + 3\frac{\left(3u_i^4 - 4\right)}{\left(\sqrt{1 + u_i^2}\right)^5\left(1 + \sqrt{1 + u_i^2}\right)^3}\right\}E\left\{u_i^2\right\} +$$
$$+ E\left\{u_i^2\frac{3\left(1 + \sqrt{1 + u_i^2}\right) + 2u_i^2}{\left(1 + u_i^2\right)\left(1 + \sqrt{1 + u_i^2}\right)^2}\right\}. \quad (9)$$

In this algorithm we use the preprocessing technique – Principal Component Analysis for whitening the observed mixture vectors.

3. Materials

In this experiment we prepared two types of the EEG recordings. In the first case, the EEG signals were recorded using the multi-channel Grass Technologies Comet EEG

system with AS40 amplifier and the digital EEG simulator. The EEG data were collected from 21 scalp electrodes with a sampling rate of 400 Hz. These waveforms include the standard EEG recordings with symmetrical eye movements, but for this experiment we added an additional sequence of the presented artifact. The real EEG signals were recorded at a 400 Hz sampling rate using a 19-electrode scalp longitudinal montage. These signals are heavily corrupted by 50 Hz line noise and muscle activity. Figure 3 and Figure 4 are shown a 5-sec interval of two types of the EEG recordings.
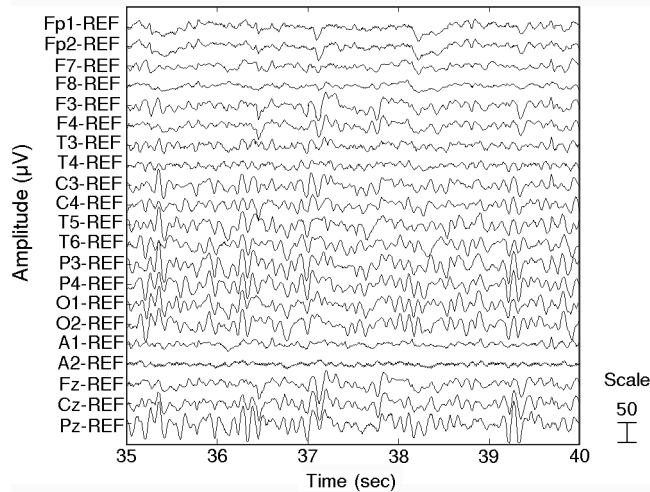
Fig. 3. The figure illustrating a set of the simulated EEG signals affected by the symmetrical eye movements (LF = 1 Hz, HF = 70 Hz)
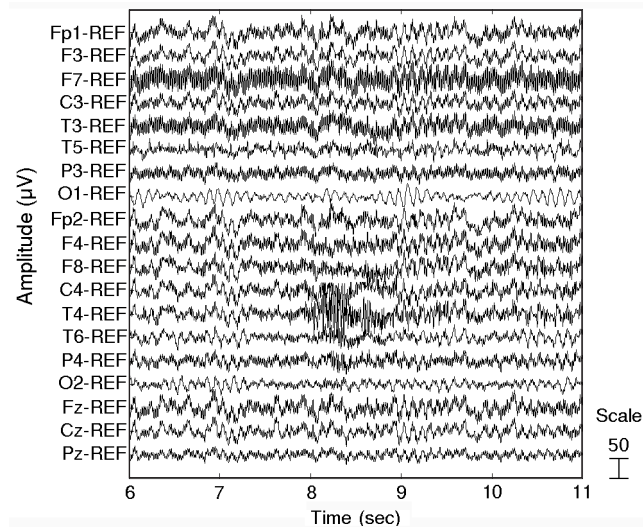
Fig. 4. The figure illustrating a set of the real EEG recordings affected by line noise and muscle activity (LF = 1 Hz, HF = 70 Hz)

The new version of the infomax approach presented in eq. 8 has been implemented in the MATLAB software using the EEGLAB toolbox [13]. The following weight update rule is used to perform ICA:

$$\Delta \mathbf{W}(n+1) = (1-\alpha)\Delta \mathbf{W}(n) + \alpha \mathbf{W}(n), \tag{10}$$

where: $\alpha > 0$. The learning rate was changed from 0.001 to 0.000002 during convergence. The accuracy was measured using the Performance Index [17] defined as:

$$\mathrm{PI} = \sum_{i=1}^{n}\left\{\left(\sum_{k=1}^{n}\frac{\left|g_{ik}\right|^2}{\max_j \left|g_{ij}\right|^2} - 1\right) + \left(\sum_{k=1}^{n}\frac{\left|g_{ki}\right|^2}{\max_j \left|g_{ji}\right|^2} - 1\right)\right\}, \tag{11}$$

where: g_{ij} – is the (i,j) element of the global system matrix $\mathbf{G} = \mathbf{WA}$, $\max_j \left|g_{ij}\right|$ – is the maximum value among the elements in the i-th row vector of $\mathbf{G}$, $\max_j \left|g_{ji}\right|$ – represents the maximum value among the elements in the i-th column vector of $\mathbf{G}$. The second proposed measure is the normalized kurtosis, which express different results of the separating process obtained by using two algorithms. Moreover, we use box plots of the PI index to compare the accuracy of two presented algorithms.

4. Results

The results of separation and elimination of the selected artifacts from the simulated and real EEG recordings are presented in Fig. 5, Fig. 6 and Fig. 7.

Figure 5A shows the ICA components obtained from a 2-sec interval of the recorded EEG time series collected from 21 simulated scalp activations using the new infomax algorithm. The two components presented by the scalp topographies are the symmetrical eye movements. Figure 5B presents the waveforms of the EEG data before and after elimination of the eye artifacts by removal of the component 1 and 3. In this figure, the results of using the infomax rule for the separation have been shown. Moreover, the analysis presented in Table 1 shows differences between values of the normalized kurtosis for two algorithms. In this experiment the eye artifacts were largely reduced, but not completely removed.

The next ICA decomposition was performed on the 3-sec EEG real data and it was used twice, because of the line noise artifact. Firstly, we removed noisy time segments presented by one component, which is shown in Fig. 6A. Components 14, 15, 17 and 19 probably represent muscle noise. Figure 6B shows the distribution of line noise power near 50 Hz in the EEG recordings. The line noise power accounted by two algorithms for was calculated by averaging power near 50 Hz in the projections of each of the 19 components. The new version of the infomax algorithm separated

the line noise power into one component, which accounted for 78.3% of this artifact in the EEG data. The extended infomax algorithm isolated the line noise artifact into the component no. 4, which composed of 74.8% of this undesired signal. The result
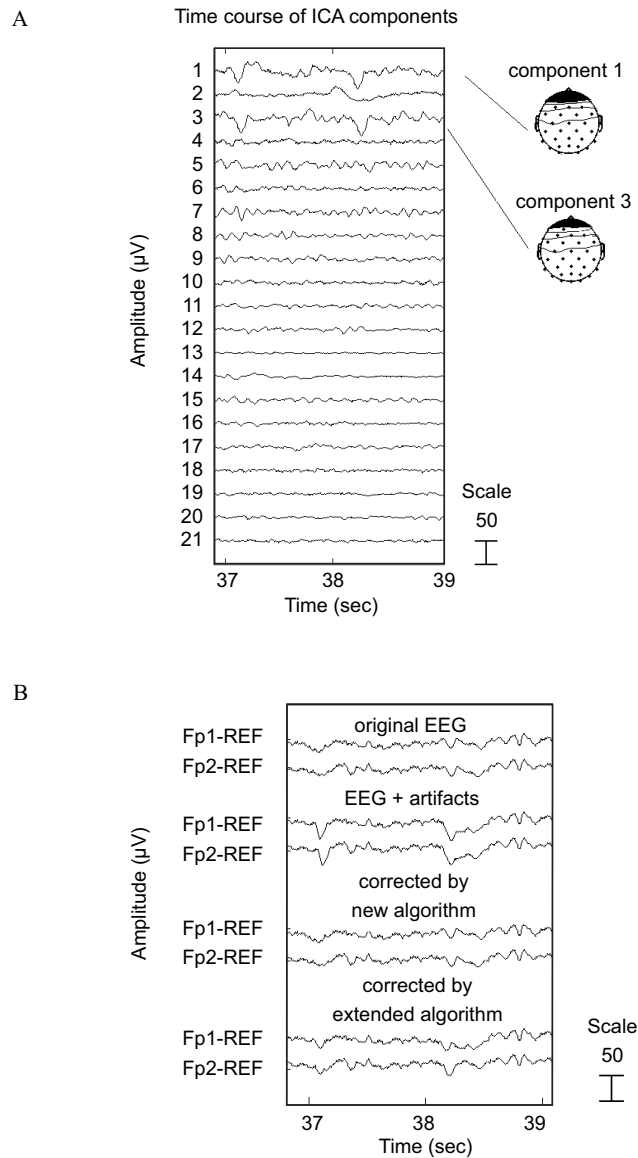
Fig. 5. Results of separation and elimination of the eye artifacts. **A.** A 2-sec interval of the ICA components extracted by the new version of the infomax algorithm and the scalp maps of two components accounting for symmetrical eye movements. **B.** Two frontal channels (Fp1-REF, Fp2-REF) before and after elimination of the eye artifacts by the extended infomax algorithm and our proposition

Table 1. The values of the normalized kurtosis before and after elimination of the symmetrical eye movements from the simulated EEG data

	Fp1-REF	Fp2-REF
original 'clean' EEG data	3.970	3.973
EEG data with artifacts	13.058	13.062
corrected by the extended infomax algorithm	4.051	4.057
corrected by the new infomax algorithm	3.972	3.975
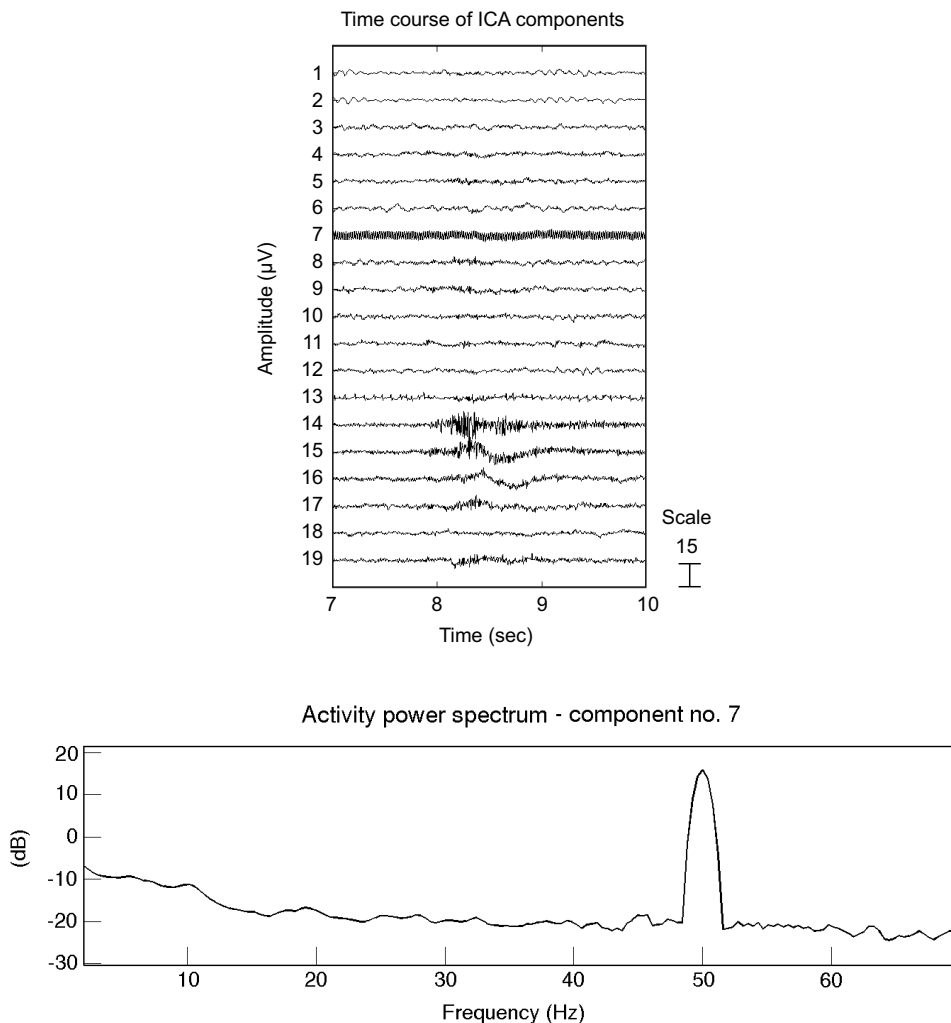
Fig. 6A. A 3-sec interval of the ICA components extracted by the new version of the infomax algorithm (top figure) and the activity power spectrum of the component no. 7 (bottom figure)
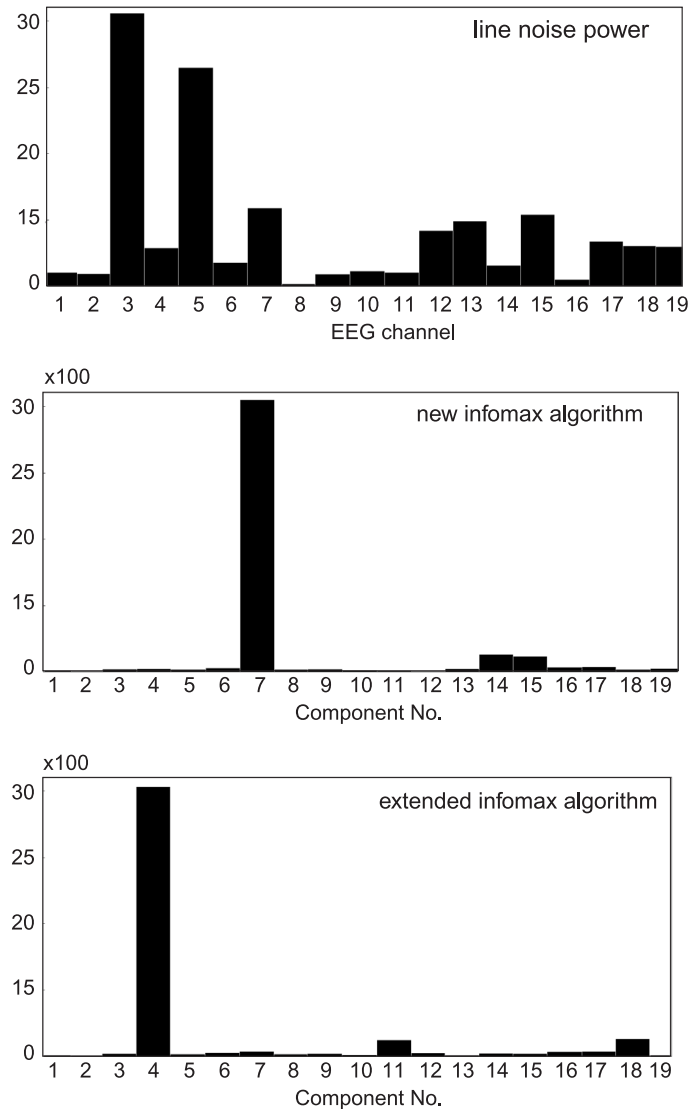
Fig. 6B. The ratio of line noise power in the EEG data (top panel) with the ICA components extracted by the new version of the infomax algorithm (middle panel) and the extended infomax algorithm (bottom panel). The vertical axis represents the ratio of power at the line frequency (50 Hz). The horizontal axis is a number of the channels or the components

of the line noise elimination by the extended infomax algorithm is almost the same like the one presented in [6]. It is worth to note, that in [6] the EEG time series was collected only from 13 scalp electrodes. The results of the line noise elimination by two adaptive algorithms can be seen in Fig. 6C.
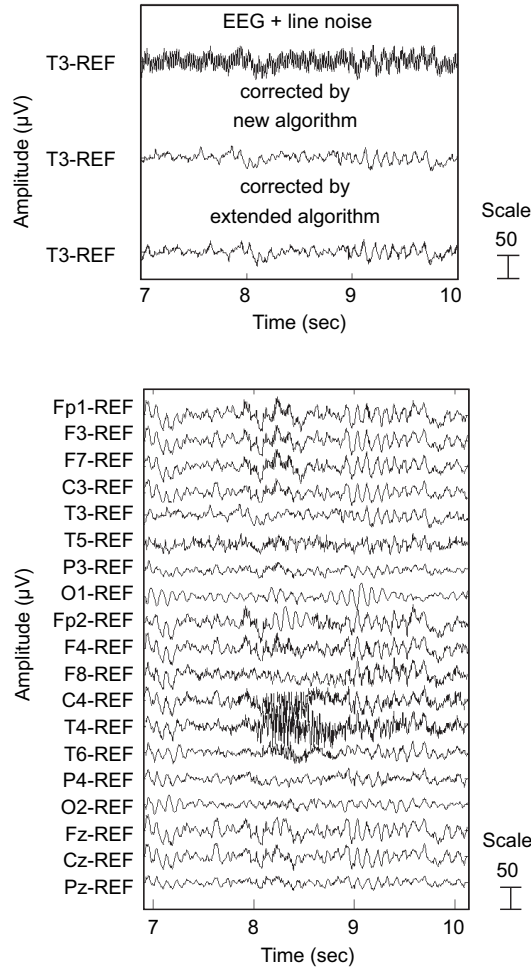
Fig. 6C. Comparison of the line noise removal by eliminating the chosen components (4 and 7), which are presented in Fig. 6B. The top figure illustrates one selected channel T3 before and after elimination the line noise artifact extracted by the extended infomax algorithm and our proposition. The bottom figure shows the all 'corrected' EEG data obtained by using the new version of the infomax algorithm

In the following step, we prepared the second decomposition. Figure 7A shows the independent components and the muscle artifacts localized between 8 and 9 sec presented by three components: 13, 14 and 19. After elimination of these components, we obtained the result illustrated in Fig. 7B. The separation carried out by the extended infomax algorithm was not precise, because in the corrected EEGs occurred a short interval of the undesired components. The differences between values of the normalized kurtosis are shown in Table 2.

A

Time course of ICA components

B
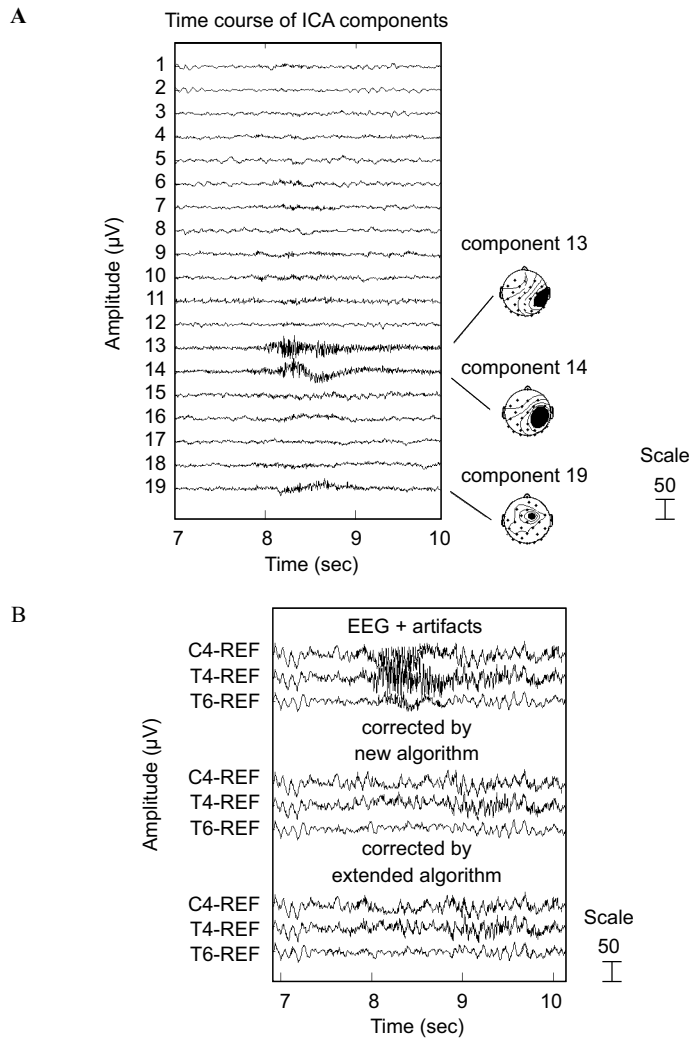
Fig. 7. Results of separation and elimination of the muscle artifacts from the real EEG data. **A.** A 3-sec interval of the ICA components extracted by the new version of the infomax algorithm and the scalp maps of three components accounting for the muscle artifacts. **B.** Three channels (C4-REF, T4-REF, T6-REF) before and after elimination of these artifacts by the extended infomax algorithm and our proposition

Table 2. The values of the normalized kurtosis before and after elimination of the muscle artifacts from the real EEG data

	C4-REF	T4-REF	T6-REF
real EEG data with artifacts	10.448	13.582	9.554
corrected by the extended infomax algorithm	3.981	4.087	3.784
corrected by the new infomax algorithm	3.758	4.079	3.702

Performance comparison between the extended infomax algorithm and our proposition is shown in Fig. 8. In ideal case, when the perfect separation is achieved, the PI index is zero. In practice, the value of this index has been changed between 10^{-4} to 10^1. It means that the adaptive algorithms separated these EEG signals quite
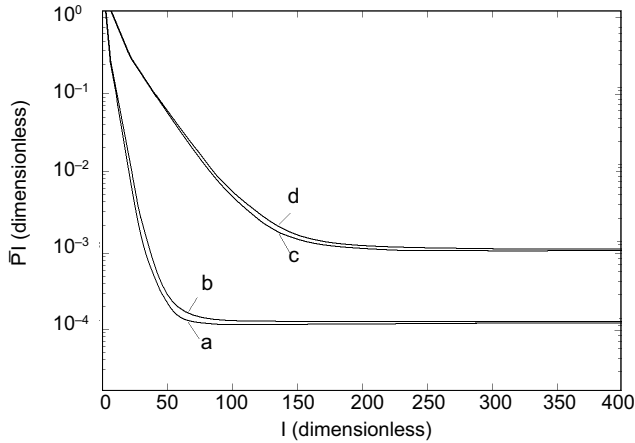
Fig. 8. The mean value of the PI index versus number of iteration for the separation of the simulated EEG recordings and the real EEG data by the new version of the infomax algorithm (a – 19 channels, b – 21 channels) and the extended infomax algorithm (c – 19 channels, d – 21 channels). The mean value of the PI index for 100 runs
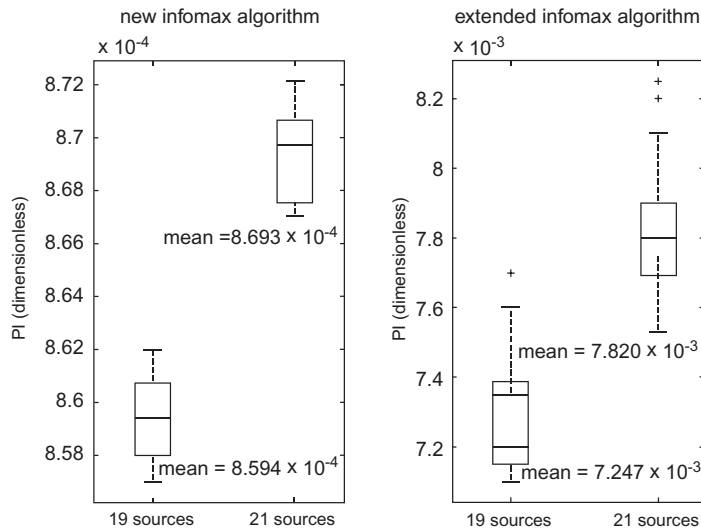
Fig. 9. Accuracy of the two natural gradient algorithms. The box plots shown differences between value of the PI index for 19 channels and for 21 channels. The mean value of the PI index depends on type of the transfer functions and number of the signals. The median and the mean values of the PI index for 100 runs. The vertical axis represents the PI index

good and it is small probability of removal of the desired brain signals. Moreover, both algorithms converge to the correct solution, but the proposed new learning algorithm converges faster than method presented in eq. 3. The differences between the mean value of the PI index of the simulated EEGs (21 channels) and the PI index of the real EEGs (19 channels) depend on the type of the transfer function and the number of signals, which are shown in Fig. 9.

5. Discussion

The success of using the presented infomax algorithm to artifact removal from the EEG data only depends on the choice of the nonlinear function $g(\mathbf{u})$, because the basic idea of the infomax rule is to match the slope of the nonlinear transfer function of the elementary processing unit in a neural network with the input PDF.

It is difficult to verify the results of eliminating artifacts from the EEG real data. Generally, it is use the visual inspection of 'clean data' or spectral plots. In [6] it has been analyzed the spectrograms of the EEG recordings before and after the elimination of activity produced by the eye movement. In addition, the new performance BCR is presented in [10]. The BCR (brain – to – contamination ratio) metric was the determinant of the correlation matrix of the original and the recovered brain and contaminant signals. However, for verification of the quality of separation of the EEGs the PI index can be proposed. Using this coefficient as a measure of accuracy is particularly simple, because the small value of the PI index gave small probability of removal of the desired brain signals. The next our proposition is the value of the normalized kurtosis, which can be used in analysis of the simulated EEG data. In the real EEG recordings, this measure shows only the differences between the results of eliminating of the artifacts obtained by using the separation algorithms, but is a very useful, when we try to compare the same algorithms with different nonlinear functions.

6. Conclusion

During the tests, it was observed that the proposed adaptive algorithm with the new nonlinearity can effectively detect the typical artifacts. Furthermore, it converges faster than the extended infomax algorithm using the parametric density model. All presented artifacts were largely reduced by using the new version of the infomax algorithm.

References

1. Majkowski J.: Clinical Electroencephalography (in Polish). Państwowy Zakład Wydawnictw Lekarskich, Warszawa 1986.
2. Fisch B.J.: EEG Primer – basic principles of digital and analog eeg, Elsevier 2000.
3. Sanei S., Chambers J.A.: EEG Signal Processing. Wiley 2007.
4. Viola F.C., Thorne J., Edmonds B., Schneiger T., Eichele T., Debener S.: Semi-automatic identification of independent components representing EEG artifact. Clinical Neurophysiology 2009, 120, 868–877.
5. Hyvärinen A., Karhunen J., Oja E.: Independent Component Analysis. Wiley, 2001.
6. Jung T.-P., Makeig S., Humphries C., Lee T.-W., McKeown M.J., Iragui V., Sejnowski T.J.: Removing electroencephalographic artifacts by blind source separation. Psychophysiology, Cambridge University Press 2000, 37, 163–178.
7. Delorme A., Sejnowski T., Makeig S.: Enhanced detection of artifacts in EEG data using higher-order statistics and independent component analysis. NeuroImage 2007, 34, 1443–1449.
8. Krishnaveni V., Jayaraman S., Gunasekaran A., Ramadoss K.: Automatic Removal of Ocular Artifacts using JADE Algorithm and Neural Network, International Journal of Computer Systems Science and Engineering 2006, 1, 322–333.
9. Chen X., Wang L., Xu Y.: A Symmetric Orthogonal FastICA Algorithm and Applications in EEG. 5th Intern. Conf. Natural Computation ICNC '09, Tianjin China, 2009, 504–508.
10. Fitzgibbon S.P., Powers D.M.W., Pope K.J., Clark C.R.: Removal of EEG Noise and Artifact Using Blind Source Separation. J. Clin. Neuroph. 2007, 24.
11. Górecka J.: Using the Independent Component Analysis for removal of undesired components from EEG data (in Polish). Inżynieria Biomedyczna, 2009, 15, 87–90.
12. Lee T.-W., Sejnowski T.J.: Independent Component Analysis for mixed sub-gaussian and super-gaussian sources. 4th Joint Symposium on Neural Computation Proc. 1997, 132–139.
13. Makeig S. et al.: EEGLAB: ICA Toolbox for Psychophysiological Research, WWW Site, Swartz Center for Computational Neuroscience, Institute of Neural Computation, University of San Diego, California, http://sccn.ucsd.edu/eeglab/.
14. Lee T.-W.: Independent Component Analysis. Theory and Applications. Kluwer Academic Publishers,1998.
15. Menon A., Mehrotra K., Mohan Ch.K., Ranka S.: Characterization of a class of sigmoid functions with applications to neural networks. Neural Networks 1996, 9, 819–835.
16. Cardoso J.F.: On the stability of source separation algorithms. The Journal of VLSI Signal Processing, Springer 2000, 26, 7–14.
17. Choi S., Cichocki A., Amari S.: Flexible Independent Component Analysis, Journal of VLSI Signal Processing – Systems for Signal. Image and Video Technology, Kluwer, 2000, 1–18.